Laboratory Experiments on Steady State Seepage-Induced Landslides Using Slope Models and Sensors

Sandra G. Catane[1], Mark Albert H. Zarco[2], Cathleen Joyce N. Cordero[1], Roy Albert N. Kaimo[1], Ricarido M. Saturay, Jr.[1]

[1]Engineering Geology Laboratory, National Institute of Geological Sciences
University of the Philippines, Diliman, Quezon City 1101
[2]Geotechnical Engineering Group, Institute of Civil Engineering
University of the Philippines, Diliman, Quezon City 1101

ABSTRACT

A thorough understanding of the failure initiation process is crucial in the development of physically-based early warning system for landslides and slope failures. Laboratory-scale slope models were constructed and subjected to instability through simulated groundwater infiltration. This is done by progressively increasing the water level in the upslope tank and allowing water to infiltrate laterally towards the toe of the slope. Physical changes in the slope models were recorded by tilt sensors and video cameras. When the model slope was destabilized, the chronology of events occurred in the following sequence: (1) bulging at the toe, (2) seepage at the toe, (3) initial failure of soil mass, (4) piping, (5) retrogressive failure, (6) formation of tension cracks and (7) major failure of soil mass. Tension cracks, piping and eventual failure are manifestations of differential settlements due to variations in void ratio. Finite element analysis indicates that instability and subsequent failures in the model slope were induced primarily by high hydraulic gradients in the toe area. Seepage, initial deformation and subsequent failures were manifested in the toe area prior to failure, providing a maximum of 36 min lead time. Similar lead times are expected in slopes of the same material as shown in many case studies of dam failure. The potential of having a longer lead time is high for natural slopes made of materials with higher shear strength thus evacuation is possible. The tilt sensors were able to detect the initial changes before visual changes manifested, indicating the importance of instrumental monitoring.

Keywords: seepage-induced landslides, landslide initiation, wireless sensors, early warning system, Philippines

INTRODUCTION

Landslides caused serious human and property losses to vulnerable communities and have contributed long-term environmental degradation. Refinement of methods and technologies in landslide hazard assessment and risk reduction has been the focus of research in the past decade. Most of these, however, are applicable to small landslides and only affluent communities are capable of installing rather expensive monitoring systems and maintaining engineering mitigating structures. In the case of massive and potentially disastrous landslides, there is no effective yet economically viable structural mitigation measure. In the end, the only options are to permanently relocate threatened communities or provide a reliable early warning system. An early warning system which is cost effective yet efficient is desired in order to make it affordable to marginalized communities, which are the most susceptible to landslides.

Existing early warning system for landslides are mostly based on instrumental monitoring of rainfall and/or distressed slopes (Mittal *et al*., 2008; Simeoni and Mongiovi, 2007; Tommasi *et al*., 2006). Parameters used in early warning systems are commonly rainfall threshold and ground deformation. In particular, rainfall thresholds have been widely used in community-based warning systems (e.g., Larsen and Simon, 1992; Guzzetti *et al*., 2007) but only limited areas have established rainfall thresholds worldwide. Moreover, landslide initiation does not solely depends on rainfall volume and intensity but also on other factors such as antecedent precipitation, fluctuations of groundwater level, geologic and topographic conditions (Tohari *et al*., 2007). Ground deformation that precedes failure has also been investigated in recent studies (Sakai, 2001; Araiba, 2006). Hong and Adler (2007) attempted to develop a real-time global satellite-based landslide prediction system based on two essential data sets, landslide susceptibility mapping and rainfall data analysis.

Potential improvement to early warning systems can be drawn from the results of laboratory experiments. The effect of changes in parameters such as moisture content (Orense *et al*., 2004; Tohari *et al*., 2007), pore-water pressure (Kuriakose *et al*., 2008), matric suction

(Huat *et al*., 2005; Gofar *et al*., 2008) and deformation (Sakai, 2001; Araiba, 2006) that leads to failure were investigated. Orense *et al*. (2004) and Tohari *et al*. (2007) found that failure of experimental slopes is preceded by an increase in moisture content.

We conducted nine laboratory experiments in a landslide box to investigate the changes in various parameters that initiate failure such as moisture content and deformation using sensors. This paper summarizes the results of the experiments such as the physical changes in the model slope and response of tilt sensors with rising water level and correlation of parameters with visual observations. A two-dimensional modeling to simulate the landslide process was also performed based on parameters used in the experiment. The result of the study is useful in identifying the most sensitive factors in an attempt to forecast landslides.

EARLY WARNING SYSTEM IN THE PHILIPPINES

The Philippines has been identified as one of the landslide hotspots in the world (Kjestad, 2007) due to its steep topography, wet climate and active tectonic setting. Among the 162 landslide-prone countries, the Philippines ranks 4th in terms of risk of human exposure to landslide and 6th in terms of potential economic loss (United Nations International Strategy for Disaster Reduction Secretariat, 2009). Disastrous landslides in the Philippines happened more frequently since 1999. These include: (1) 1999 Cherry Hills landslide in Antipolo, (2) 2003 Panaon Island-Surigao flooding landslides, (3) 2004 Aurora-Quezon flooding landslides, (4) 2006 Guinsaugon landslide in Southern Leyte, (5) 2006 Mayon lahars in Albay (Catane, *et al.*, 2008). About 3,000 loss of lives and billions of pesos of property damage were incurred by these events. All the above mentioned landslides were preceded by heavy rainfall but no prior monitoring and early warning system were in place. The high casualty and enormous property damage highlight the need for an early warning system, especially in high-risk areas.

Soon after the Panaon disaster in 2003, the Philippine government launched the National Geohazards Mapping Program. Landslide susceptibility maps of 1:50,000 scale were produced for the entire country. More recently, a

multi-agency program called Hazards Mapping for Effective Community-Based Disaster Risk Management (READY) was implemented at the local level (NDCC, 2008). The program has been conducted in 27 selected and high risk Philippine provinces. One of the components is community-based disaster risk mitigation using community-based early warning system (CBEWS). Meanwhile, various non-government organizations (NGOs) such as Manila Observatory (MO), Center for Environmental Concerns (CEC), CARE Philippines and Center for Disaster Preparedness (CDP), have organized local communities affected by landslides (e.g., Aurora-Quezon, Guinsaugon and Legaspi). Early warning system is an integral part of their programs.

Current early warning systems in the Philippines are underdeveloped since values for rainfall threshold is based on limited instrumental and historical data, or global values rather than site-specific values. Moreover, since the relation between rainfall and landslide occurrence is empirically determined and site-specific, threshold values established for an area could not always be applied to other areas. Thus, the relation of rainfall to landslide initiation needs further clarification.

An effective early warning system requires full understanding of landslide triggering process prior to failure. A research program, Disaster Risk Management Using Sensors, Networks and Computing: Early Warning System for Landslides, Slope Failures and Debris Flows (DRMS), was conceived to investigate landslide initiation on model slopes using wireless sensor networks (WSN). This research program aims to develop an alternative means for monitoring slopes that is both cost effective yet efficient. It is a collaborative research between the College of Engineering and College of Science of the University of the Philippines, Diliman.

METHODS

A landslide box was used to reproduce seepage-induced failure where slope geometry and soil properties were kept constant in all the experiments except for Experiment 1 where loose soil was used. Sensor columns were inserted in the upper slope and in the toe. Initial condition on water level was established after which water column was raised at an approximate rate of 10 cm/10 min to 10 cm/15 min until the water level reached 115 cm. Given the initial conditions and observations, a numerical model simulation was performed to check the consistency of the results.

Soil Sample

The soil used to construct the model slopes in the experiments is *Porac sand* obtained from Porac river, Pampanga Province. Porac sand is a lahar deposit derived from Pinatubo volcano. It is composed of plagioclase, quartz and ferromagnesian minerals. To improve the homogeneity of the sample, it was sieved using a 1 mm wire mesh to remove greater than 1 mm coarse fraction. The specific gravity of the soil is 2.67. The maximum and minimum void ratios are 0.918 and 0.699, respectively (Orense *et al.*, 2006). Loose soils used in Experiment 1 represent behavior for high void ratio whereas dense soils used in experiments 2 through 9 represent behavior for low void ratio.
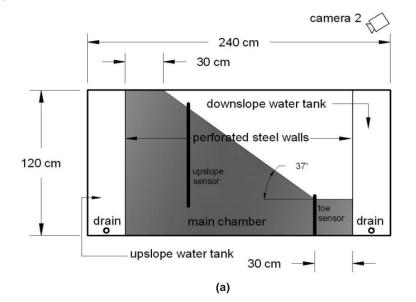
Landslide Box

The landslide box, shown in Fig. 1a, is 240 cm long, 90 cm wide and 120 cm high. Its walls, except for one, are made of steel plates. A transparent plexi glass was used in one of the side walls to visually observe changes in the model slope.
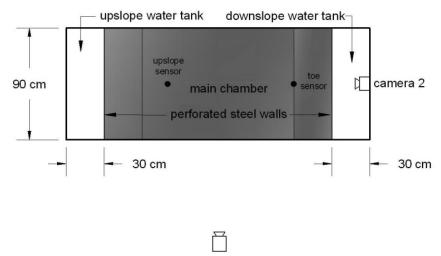
The box is divided into three sections: the upslope water tank, the downslope water tank and the main chamber (Fig. 1a). The water tanks are 30 cm x 90 cm while the main chamber is 180 cm x 90 cm. Separating the said chambers are perforated steel walls covered with wire mesh. The walls allow water to pass through without flushing out the sand grains. A plastic hose was used to fill in the upstream water tank. Faucets are installed at the bottom of the water tanks to control water outflow.

The plexiglass and steel side panels were lubricated using petrolatinum jelly to minimize the friction between the panel and the soil. This resulted in a condition in which shear stresses were assumed to be negligible. The side panels were considered to be rigid such that

no deformation in the direction perpendicular to the wall resulting in negligible out-of-plane strains. Also, the impermeable side panels prevented flow perpendicular to the wall which made the seepage two dimensional. The perforated panels at the upslope and downslope were assumed to be completely pervious such that the hydraulic head at these boundaries were assumed equal to that in the tanks. These boundaries were also assumed to be sufficiently rough and rigid so as to prevent displacements both in the vertical and horizontal directions.

Monitoring Sensors

Sensor columns containing several nodes for measuring tilt are installed at the upper slope and at the toe of the model slope. The nodes with a sampling interval of 1 sec measure acceleration and transmit collected data to a central repository computer. The data is converted to tilt angle and analyzed for ground deformation. The details of the sensor column development were described in De Dios *et al.* (2010).
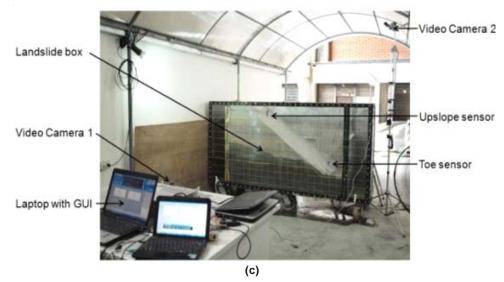

(a)

(b)

Figure1. Schematic diagram of the landslide box used in the experiments. (a) section view and (b) plan view. (c) laboratory set-up showing the landslide box, sensors and data acquisition system.

Visual Monitoring

Two video cameras were set-up to monitor the changes in the model slope such as development and movement of wetting front and deformation. Camera 1 is positioned to monitor the cross-section and Camera 2 is placed in front of the slope face. Camera 2 provides a more detailed view of the saturation process, movement of the soil mass and failure sequence. This visual monitoring set-up facilitated correlation of tilt sensor readings and visual observations.

Initial Conditions

Except for Experiment 1, where the soil was loosely placed, the model slopes were constructed in the main chamber and were manually compacted in lifts of 10 cm thickness. The first three layers of soil were spread uniformly on the surface of the chamber to form the base of the slope. The final dimension of the slope was 90 cm high and 120 cm wide with a slope angle of 37°. After constructing the model slope, the upslope tank was filled gradually with water up to the 40 cm mark. Water was allowed to seep through the soil and percolate laterally towards the downslope tank. Initial condition was set at 40 cm and 20 cm water level at the upslope and downslope tanks, respectively. In the series of experiments, it took 3 to 7 hours to establish the initial conditions.

The experiment proceeded by increasing water inflow in the upslope tank while keeping the 20 cm mark in the downslope tank. To initiate failure by seepage, the water level in the upstream tank was increased at a rate of 10 cm/10 min from L=40 cm to L=80 cm then 10 cm/15 mins from L= 80 cm until the head of the slope collapses. This condition is steady-state seepage. In the real world, this set-up closely resembles a steady-state flow of groundwater in (1) natural slopes, and (2) accumulation of water behind natural landslide debris dams and earth dams used in containing mine tailings. The experiment is completed when no further failure is observed.

Finite Element Modeling

A two-dimensional elastoplastic finite element modeling of the landslide box was performed using RocScience Phase^2 software to determine which factors significantly affect the failure of the slope. The soil mass was assumed homogenous and isotropic. It has a permeability of $k=1\times10^{-3}$ cm/sec, a Young's modulus of E=15 MPa, and a Poisson's ratio of v=0.3 based on laboratory tests performed on the same material type and void ratio (Zarco *et al.*, 1999). Based on direct shear strength tests performed on reconstituted samples, the Mohr Coulomb parameters, effective friction angle (ϕ'=34°) and effective cohesion (c'=0.001 MPa) for a sample with a saturated unit weight of 18

kN/m^3 were used for the analyses. The mesh used consisted of 175 6-node interpolated triangular elements. This mesh provides the optimum solution as further refinement of the mesh will not significantly change the results.

The problem was analyzed as plane strain problem in which the resistance between the soil and the walls of the landslide box was considered negligible. Details regarding the implications of this assumption in comparison with experimental results are given in the section under Discussion.

The loading sequence consisted of computing the in-situ state of stress from gravity loads, then increasing the height of the water in the upslope water tank in seven stages to a height of $h_0 = 0.3$ m, 0.6 m, 0.75 m, 0.9 m, 0.95 m, 1.0 m, and 1.07 m.

RESULTS

We conducted a total of 9 experiments (Experiment 1 to 9) using similar conditions. Appropriate initial conditions for the slope model were tested while tilt, pore-water pressure and soil moisture sensors (De Dios *et al*., 2010) were tested and calibrated in the first 6 experiments. The subsequent experiments, 7, 8 and 9 produced consistent and reasonable results. Only visual monitoring and tilt measurements were used in the last three experiments because the other sensors still need calibration and refinement. Experiment 7 is described in detail in this paper. Experiments 8 and 9 produced similar results, which demonstrate the repeatability of the experiment. Although details of each experiment were unique, the results and sequence of events were consistent in the last three experiments. Table 1 summarizes water levels, significant events and sensor reading changes.

Development of the Saturation Zone

In order to establish the initial conditions, water was allowed to seep through the perforated steel wall and migrate laterally toward the downslope tank, producing a saturation zone. The profile of the wetting front is asymmetric as shown in Fig. 2. A capillary zone has developed adjacent to the upslope tank which resulted to the higher level of the saturation zone than the water level in the upslope tank. When the initial conditions were attained, the experiment was set to commence at $T_0=0$.

When the water level was increased, the saturation zone rose and expanded laterally. Seepage occurred at the toe when the water level in the upslope water tank reached 70 cm at $T_1=30$ min.

The first movement of the soil mass was observed after 44 min (T_2) when almost half of the slope face was saturated. The water level at this time was 84 cm.

Piping at the sand/wall interface began at $T_3=53$ min at 90 cm water level (Fig. 3). At $T_4=94$ min, water from the upslope tank flooded the main chamber due to retrogressive failure of the slope.

Slope Deformation

Movement of the soil mass was preceded by the development of bulges or pressure ridges at the toe area at $T_{1d}=21$ min and water level of 61 cm (Fig. 4).

Minor failures of the slope in the form of surface erosion occurred at $T_{2d}=44$ min and water level of 84 cm. These movements marked the onset of retrogressive failure. Meanwhile, a sand slurry was formed at the base of the slope when seepage water was absorbed in the failed soil mass.

Tension cracks started to form in the unsaturated portions of the slope face. The first tension crack was observed at $T_{3d}=71$ min and a water level of 99 cm. A series of failure occurred along the cracks. The largest tension crack appeared near the head of the slope (Fig 5). The failure of the soil mass along this crack happened at $T_{4d}=81$ min.

The experiment was terminated at $T_{5d}=94$ min when the head of the slope finally collapsed and water surged from the upslope tank.

Correlation with Sensors

The nodes in the sensor column installed at the toe area show changes in tilt up to 0.9 deg (Fig. 6). Movements were detected 14 to 22 min prior to the

Table 1. Correlation of water levels, significant events and sensor reading changes

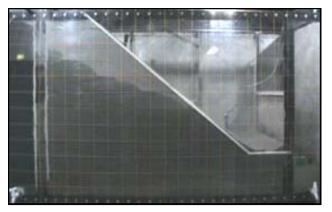| Time (min)	Upslope Tank Water Level (L) (cm)	Visual Observation: Saturation Zone	Visual Observation: Deformation	Toe Sensor Reading	Upslope Sensor Reading
0	40	T_0: Establishment of initial condition	T_0: Establishment of initial condition	T_0: Establishment of initial condition	T_0: Establishment of initial condition
8	48			$T_{n3.1}$: Initial change in tilt in toe sensor node 3	
21	61	------	T_{1d}: Bulging at the toe	------	------
22	62	------	------	$T_{n3.2}$: Change in tilt in toe sensor node 3	------
30	70	T_1 : Formation of seepage area at the toe	------	------	------
31	71	------	------	T_{n1}: Change in tilt in toe sensor node 1	------
40	80	------	------	T_{n2}: Change in tilt in toe sensor node 2	------
44	84	T_2: Initial movement of soil mass	T_{2d}: Initial movement of soil mass	------	------
53	90	T_3: Piping	------	------	------
55	90	------	------	------	T_{n4}: Change in tilt in upslope sensor node 4
60	93	------	------	------	T_{n5}: Change in tilt in upslope sensor node 5
62	94	------	------	------	T_{n6}: Change in tilt in upslope sensor node 6
63	95	------	------	------	T_{n1}: Change in tilt in toe sensor node 1
64	96	------	------	------	$T_{n3}=T_{n7}$: Change in tilt in upslope sensor nodes 2 and 7
65	96	------	------	------	T_{n3}: Change in tilt in upslope sensor node 3
71	99	------	T_{3d}: First tension crack appears	------	------
81	110	------	T_{4d}: Major failure of soil mass	------	------
93	113	T_4: Water from the upslope tank flooded the main chamber	T_{5d}: Head of the slope collapsed	------	------

Figure 2. Profile of the asymmetric wetting front at 80 cm water level.

Figure 3. Piping at the toe of the slope model (view from Camera 2).
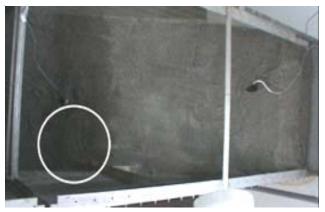

Figure 4. Bulging at the toe (view from Camera 2).

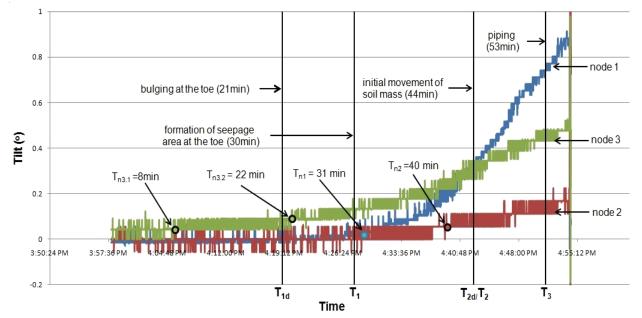Figure 5. Plan view of the largest tension crack just above the upslope sensor column. (view from Camera 2).

Figure 6. Toe sensor readings. All nodes have positive tilt (node tilts away from the slope).

visually observed seepage at the toe and 9 to 13 min before bulging manifested. In Experiment 7, the sensors detected the initial tilt 36 minutes before the first failure (T_{2d}) and 72 minutes before the major failure (T_{4d}) of the slope.

The upslope sensors did not detect any of the earlier movements in the toe area. However, changes were recorded when movements progressed to the upper portion of the slope model but prior to the main failure (Fig. 7).

Finite Element Modeling

Results of the analyses for each stage are illustrated in Fig 8. As shown in the figures, progressive saturation of the slope results in a vertical downward displacement of the top of the slope, followed by lateral bulging at the toe of the slope beginning at $h_0 = 0.75$ m (Fig. 8d). The bulging continued to increase as the head in the upstream water tank was increased until failure occurred at $h_0 = 1.07$ m (Fig. 8h). The bulging continued to increase as the head in the upstream water tank was increased until failure occurs at $h_0 = 1.07$ m (Fig. 8h). Also noticeable was the development of very high hydraulic gradients in a localized zone at toe area of the slope which indicates the presence of large seepage forces locally occurring in this area. During numerical experiment, the hydraulic gradient in the toe zone has

increased from 0.7 when initial bulging occurs in the toe zone at $h_0 = 0.7$ m to a maximum value of 0.96 when failure occurs at $h_0 = 1.07$ m. These values are within the critical hydraulic gradient required to cause erosion and piping which is estimated to be within range of 0.87 to 1.06 based on the given range of void ratios of the material.

Figure 9 illustrates the predicted conditions within the slope during failure at $h_0 = 1.07$ m. The finite element mesh together with the enforced boundary seepage and deformation boundary conditions is shown in Fig. 9a. Figure 9b shows the corresponding deformed mesh and displacement vectors at the initiation of failure, while Fig. 9c is a contour plot showing the variation of the shear strain within the slope during failure. Figures 9b and 9c indicate a rotational type failure for the slope. Figure 9d is a contour plot of the pore pressure distribution within the slope. Comparing this figure with corresponding Fig 8h, failure in the slope occurs primarily due to high hydraulic gradients that resulted in large seepage forces, rather than the decrease of shear strength resulting from high pore pressures.

In Experiments 2 through 9 where the slope model was constructed by placing and compacting material in layers as previously described in the Methods, no significant vertical settlements or slumping was observed with increasing water level. Slumping at the
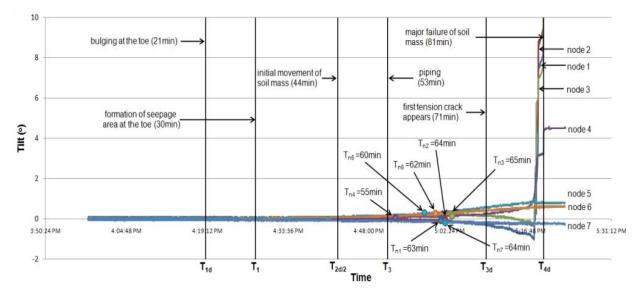

Figure 7. Upslope sensor readings from T_{1d} to T_{4d}. Positive tilt values=node tilts away from the slope; negative tilt values=node tilts towards the slope.
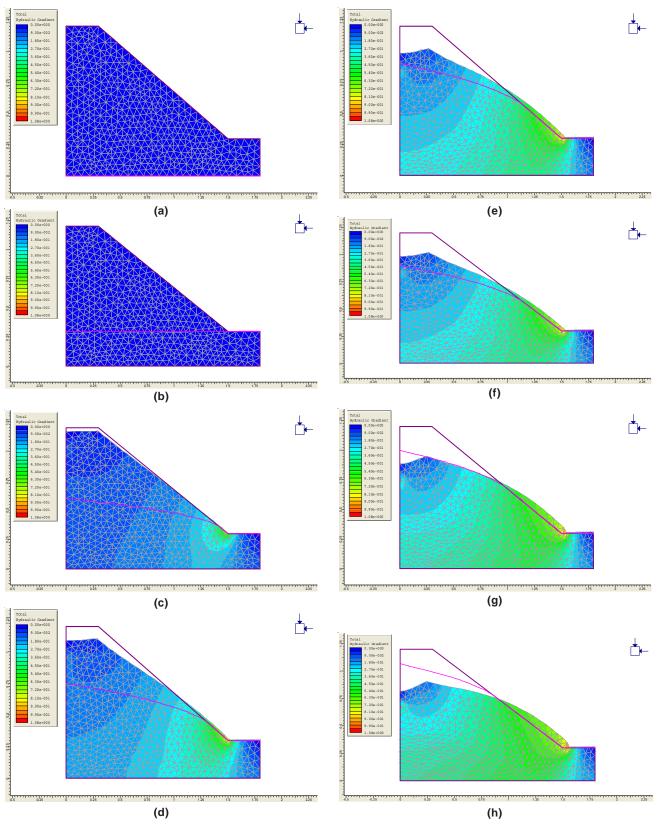
Figure 8. Contour plot showing the change in hydraulic gradient distribution within test embankment with increase in upstream head. (a) Initial gravity load, (b) h_0=0.3 m, (c) h_0=0.6 m,(d) h_0=0.75 m, (e) h_0=0.9 m, (f) h_0=0.95 m, (g) h_0=1.0 m, (h) h_0=1.07 m.

toe was noticed only when the critical hydraulic gradient was reached. Furthermore, the failure surface was observed to be shallow and elongated in shape.

In Experiment 1, where the material was loosely placed during construction of the slope model, significant vertical settlements at the crest together with slumping of the slope were observed as the water level increased. The failure mechanism was observed to be deep seated with a circular-shaped failure surface. These observations are consistent with that predicted by the numerical simulation. It is noteworthy that deformations during the increase of water level are predominantly inelastic, i.e. these deformations are permanent.

The differences in the observed movements and the failure mechanism described above can be attributed to the dilative behavior of dense or stiff soils upon shearing (Roscoe *et al.*, 1958). During shearing at failure, this dilative tendency results in resistance

between the soil and the landslide box. This resistance increases with depth within the slope model. At the surface where the soil is not confined, the resistance along the sides of the landslide box is less. This phenomenon can be simulated in the numerical model by including side resistance as upward vertical body force proportional to the vertical stress at a given point. For numerical simulations of experiments 7 through 9, imposing a body force corresponding to 80% of the vertical stress results in similar displacements and failure mechanism with that obtained experimentally.

DISCUSSIONS

The slow infiltration of water into the soil mass has led to the initiation of various phases of slope failure. The formation of bulges or pressure ridges, seepage and surface erosion at the toe area were all related to the development of very high hydraulic gradients, which indicates the presence of large seepage forces locally occurring in this area.
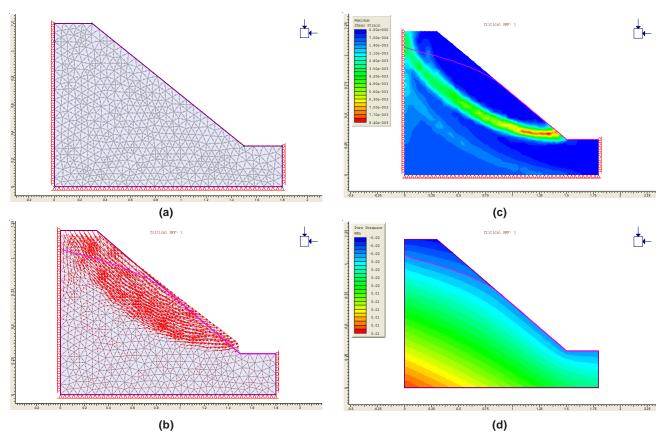

Figure 9. Results of finite element analysis of landslide box experiment summarizing conditions at failure. (a) finite element mesh, (b) deformed mesh and displacements vectors at failure, (c) contour plot of shear strain profile at failure, (d) contour plot of pore pressures at failure.

This condition was first captured by the toe sensor node 3 at t=30 min and water level of 70 cm (Fig. 6). The above result justifies the importance of installing sensors at the toe of slopes since they are most sensitive to changes.

Finite element modeling predicted the very high hydraulic gradients (Fig. 8) rather than the reduction of shear strength resulting from high pore pressures as the main mechanism for failure. High hydraulic gradients are physically manifested by pressure ridges, seepage and surface erosion. The modeling confirms that the appropriate site for installation of monitoring instrument and sensors is the toe area to capture the changes in hydraulic gradients.

Initial failure of the toe caused the removal of support and increased the slope angle and consequently resulted to retrogressive failure. The change in tilt in upslope sensor nodes 1 to 7 are all related to retrogressive failure (Fig. 7).

Tension crack is an extension fracture caused by tensile stress. It reduces the overall stability of a slope by decreasing the shear strength. Even before the tension cracks manifested, all nodes in the upslope sensor column have detected change in tilt (Fig. 7).

In natural slopes, abrupt variations in void ratio naturally occur. The experiments highlight the differences in settlement patterns and failure mechanisms due to these variations. The key implication to this is that large differential settlements can occur during saturation which then can cause fracturing, giving rise to conditions ideal for piping, erosion and eventual slope failure.

Lead times in large scale embankments are expected to be similar to those in the laboratory model. Based on documented failures of large-scale earth dams, the time between initiation of piping and embankment failure is generally in a matter of a few hours. For example, in the case of the Teton dam (Idaho, USA) and Baldwin Hills dam (California, USA) failure, the lag time was 4-4.5 hrs and 2-3 hrs, respectively (Randle *et al.*, 2000).

Laboratory experiments indicate that instrumental and visual observations of deformation are useful indicators of impending failure apart from changes in saturation, which was visually observed.

In many landslides, precursors such as appearance of seepage, deformation at the base of the slope and the formation of tension cracks were observed prior to failure. Similar features were noted in the experiments even if the conditions in natural slopes are more complex due to variability of earth materials and seepage conditions. Although the lead time for physical changes is rather short in the experiments, the potential of having a longer lead time is high for natural slopes made of materials with higher shear strength.

CONCLUSION

The toe area manifests the most significant visual and instrumental measurement changes. The physical changes observed such as pressure ridges, seepage and surface erosions are indications of high hydraulic gradients as demonstrated by the finite element modeling. Differences in void ratio give rise to differential settlements in the slope that manifest as fractures, piping and eventual failure. A maximum of 36 min lead time prior to failure is possible for a slope of the same soil properties, geometry and initial conditions. Similar lead times have been observed to occur in large scale embankments.

The initial result of this study indicates that instrumental and visual observations of deformation are useful indicators of impending failure apart from changes in saturation and pore-water pressure. Indeed, initial changes in the model slope were detected by the sensors highlighting their importance in monitoring and prediction. Instrumental monitoring of the upper part of the slope is not as significant as those observed in the toe since the deformation features appeared only after failure has started. However, monitoring the upper slope is still recommended because changes occurred prior to the main failure, which is the most disastrous phase in the evolution of a landslide.

ACKNOWLEDGEMENT

REFERENCES

Araiba, K., 2006. Study on the method for detecting and monitoring of pre-failure deformation in slope. *Disaster mitigation of debris flows, slope failures and landslides* 2: 581-589

Catane, S.G., Zarco, M.A.H. and Saturay, R.M., 2008. Landslide-Risk Reduction Strategies and Practices in the Philippines: *In: The Proceedings of the First World Landslide Forum, Tokyo, Japan.*

De Dios, R.J., Enriquez, J., Victorino, F.G., Mendoza, E.A.V., Talampas, M.C. and Marciano, J.J.Jr. 2010. A tilt, soil moisture, and pore water pressure sensor system for slope monitoring applications. *Science Diliman* 21: 15-27.

Gofar, N., Lee, M.L. and Kassim, A., 2008. Response of Suction Distribution to Rainfall Infiltration in Soil Slope. *Electronic Journal of Geotechnical Engineering 13: 1-13.*

Guzzetti, F., Perucacci, S., Rossi, M. and Stark, C. P., 2008. The rainfall intensity–duration control of shallow landslides and debris flows: an update. *Landslides* 5: 3-17.

Hong, Y., Adler, R. and Huffman, G., 2006. Evaluation of the potential of NASA multi-satellite precipitation analysis in global landslide hazard assassment. *Geophysical Research Letters* 33: L22402, doi:10.1029/2006GL028010.

Huat, B.B.K., Ali, F.Hj. and Mariappan, S., 2005. A study on suction-rainfall response of a cut slope in unsaturated residual soil using a field rain simulator. *American Journal of Environmental Science* 1: 11-15

Kjekstad O., 2007. The challenges of landslide hazard mitigation in developing countries. *1st North American Landslide Conference, Vail, Colorado, 3-8 June 2007.*

Kuriakose, S.L., Jetten, V.G., van Westen, C.J., Sankar, G. and van Beek, L.P.H, 2008. Pore water pressure as a trigger of shallow landslides in the western Ghats of Kerala, India: some preliminary observations from an experimental catchment. *Physical Geography* 29: 374-386.

Larsen, M. C., and Simon, A., 1992. A rainfall intensity-duration threshold for landslides in a humid-tropical environment, Puerto Rico [abs] *Geological Society of America: Abstracts with programs* 24: A234.

Mittal, S.K., Singh, M., Kapur P., Sharma B.K. and Shamsi, M.A., 2008. Design and development of instrumentation network for landslide monitoring and issue on early warning. *Journal of Scientific and Industrial Research* 67: 361-365.

National Disaster Coordinating Council (NDCC) 2008. Hazards mapping for effective community-based disaster risk mitigation (READY) Project. *In: the Proceedings of the International Conference-Workshop on the 17 February 2006 Guinsaugon landslide, Philippines*: 27.

Orense, R.P., Shimoma, S., Maeda, K. and Towhata. I. 2004. Instrumented model slope failure due to water seepage. *Journal of Natural Disaster Science* 26: 15-26.

Orense, R.P., Zapanta, A. Jr., Hata, A. and Towhata, I., 2006. Geotechnical characteristics of volcanic soils taken from recent eruptions. *Geotechnical and Geological Engineering* 24: 129-161.

Randle, T. J., Bountry, J. A. Kiling, R. and Lockhart, A., 2000. Geomorphology and River Hydraulics of the Teton River Upstream of Teton Dam, Teton River, Idaho. Bureau of Reclamation, US Department of the Interior. 48 p.

Roscoe, K. H., Schofield, A. H. and Wroth, C. P., 1958, On the yielding of Soil. *Geotechnique*. Vol 8, pp 22-53.

Sakai, H., 2001. Observation of ground displacement in landslide by monitoring groundwater composition. *Quarterly Report of RTRI* 42: 161-167.

Simeoni, L. and Mongiovi, L., 2007. Inclinometer monitoring of the Castelrotto landslide in Italy. *Journal of Geotechnical and Geoenvironmental Engineering* 133: 653-666.

Tohari, A., Nishigaki, M., and Komatsu, M., 2007. Laboratory rainfall-induced slope failure with moisture content measurement. *Journal of Geotechnical and Geoenvironmental Engineering* 133: 575-587.

Tommasi, P., Pellegrini, P., Boldini, D. and Ribacchi, R., 2006. Influence of rainfall regime on hydraulic conditions and movement rates in the overconsolidated clayey slope of the Orvieto hill (central Italy). *Canadian Geotechnical Journal* 43(1): 70-86.

United Nations International Strategy for Disaster Reduction Secretariat (UNISDR), 2009. Global Assessment Report on Disaster Risk Reduction [Online] Available: http://www.preventionweb.net/english/countries/statistics/risk.php?cid=135 [Accessed October 6, 2009]

Zarco, M. H., Parayno, F. C., Tuibeo, L. L. S., Papa, J. R. P. Jr., and de Leon, G. R. 1999. Geotechnical properties of redeposited lahar derived from the 1991 Mt. Pinatubo Eruption. *Terminal Report to PCIERD-DOST*. Technical Report No., UP/BRS-1-1-99.